Energy Transmission Transformer for a Wireless Capsule Endoscope: Analysis of Specific Absorption Rate and Current Density in Biological Tissue

Kenji Shiba*, *Member, IEEE*, Tomohiro Nagato, Toshio Tsuji, *Member, IEEE*, and Kohji Koshiji, *Member, IEEE*

***Abstract*—Thispaper reports on the electromagnetic influences on the analysis of biological tissue surrounding a prototype energy transmission system for a wireless capsule endoscope. Specific absorption rate (SAR) and current density were analyzed by electromagnetic simulator in a model consisting of primary coil and a human trunk including the skin, fat, muscle, small intestine, backbone, and blood. First, electric and magnetic strength in the same conditions as the analytical model were measured and compared to the analytical values to confirm the validity of the analysis. Then, SAR and current density as a function of frequency and output power were analyzed. The validity of the analysis was confirmed by comparing the analytical values with the measured ones. The SAR was below the basic restrictions of the International Commission on Nonionizing Radiation Protection (ICNIRP). At the same time, the results for current density show that the influence on biological tissue was lowest in the 300–400 kHz range, indicating that it was possible to transmit energy safely up to 160 mW. In addition, we confirmed that the current density has decreased by reducing the primary coil's current.**

***Index Terms*—Capsule endoscope, International Commission on Nonionizing Radiation Protection (ICNIRP), current density, energy transmission, specific absorption rate (SAR).**

I. Introduction

THERE has been a great deal of recent progress in the development of wireless capsule endoscopes for taking video images of digestive organs [1]–[8]. M2A [1] (Given Imaging, Ltd.) and Endo Capsule [2] (Olympus Corporation) are commercially available systems for this purpose. These systems are very small, measuring 26 mm in length and 11 mm in diameter.

However, this type of system is unable to take videos or inspect the whole gastrointestinal tract in detail because of time restraints for filming (8 h, 2 frames/s) imposed by operating with internal batteries. Thus, methods for supplying energy from outside the body to a capsule endoscope have been proposed to extend the operating time of these systems. One of these methods involves transmitting energy using electromagnetic induction between two coils placed inside and outside the body [9]–[12]. However, for practical application of this method, it is necessary to investigate the electromagnetic influence of the energy transmission system on biological tissue.

Electromagnetic influences on biological tissue include thermal effects and stimulant action. The former is the effect of generating Joule heat on biological tissue, and the latter involves exciting neurons and muscles by the induced current. The specific absorption rate [SAR, watts per kilogram (W/kg)] [13], [14] is often used as an index of the thermal effects, and current density, ampere per square meter $(\mathrm{A/m^2})$, is often used as an index of the stimulant action.

Research on the effects of SAR and current density on biological tissue when radiated with an electromagnetic field includes studies of energy transmission apparatus for artificial hearts [15]–[18] and apparatus for transcranial magnetic stimulation [19]. For example, Schuder *et al.* used numerical integration to estimate the power loss in the tissue surrounding an air-core transcutaneous transformer for an artificial heart [15]. However, their method was not a detailed estimation, but rather a simple calculation, which treated the biological tissue as a homogeneous substance. Shiba *et al.* [16]–[18] numerically analyzed the SAR in the biological tissue surrounding an externally coupled transcutaneous transformer and air-core transcutaneous transformer for an artificial heart using the transmission-line modeling (TLM) method [18], [20]–[23]. In these studies, it was possible to transmit power with high efficiency (90%–98%) because the transmission distance was short (about 5 mm) and the coils were large (ϕ: 70 mm $\times$ 5 mm) and fixed in position. In the system for the capsule endoscope, however, it is necessary to use an electromagnetic larger field because the transmission distance is large (about 100 mm or more) and the coils are very small ($<\phi$: 11 mm $\times$ 26 mm). Therefore, it is necessary to conduct an investigation focusing on the capsule endoscope.

In this paper, to determine the appropriate transmission conditions (frequency and output power) to reduce the electromagnetic influences on biological tissue, we analyzed the localized SAR (average value of biological tissue 10 g) and current density on biological tissue surrounding a primary coil for transmitting power by an electromagnetic simulator using the TLM method. We also measured the electric and magnetic fields with a biological phantom in an actual environment and compared the results with the analytical values to determine whether analytical values derived by the electromagnetic simulator are correct.

II. Energy Transmission System

A wireless capsule endoscope with an energy transmission system consists of an image transmitter, an image sensor, LEDs,

Manuscript received June 27, 2007; revised October 10, 2007. *Asterisk indicates corresponding author.*

*K. Shiba is with the Graduate School of Engineering, Hiroshima University, Higashi-Hiroshima 739-8527, Japan (e-mail: shiba@bsys.hiroshima-u.ac.jp).

T. Nagato and T. Tsuji are with the Graduate School of Engineering, Hiroshima University, Higashi-Hiroshima 739-8527, Japan (e-mail: nagato@bsys.hiroshima-u.ac.jp; tsuji@bsys.hiroshima-u.ac.jp).

K. Koshiji is with Tokyo University of Science, Chiba 278-8510, Japan (e-mail: koshiji@ee.noda.tus.ac.jp).

Digital Object Identifier 10.1109/TBME.2008.919721

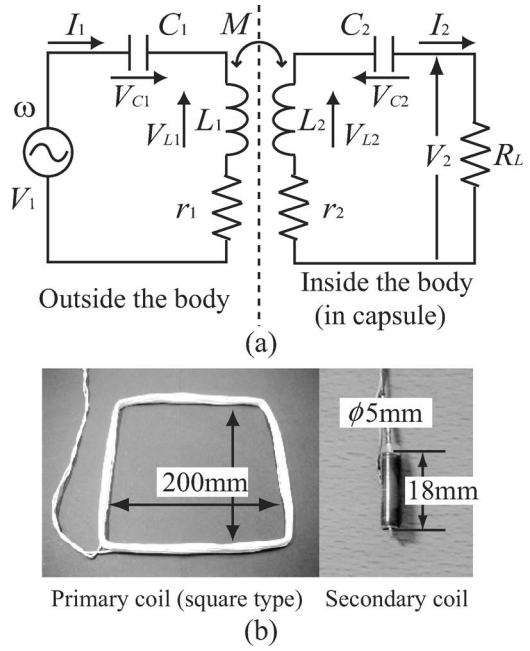

Fig. 1. (a) Equivalent circuit of the energy transmission system. (b) Coils for energy transmission.

electronics circuit, and receiver coil (secondary coil). According to recent reports, these devices require a power input of about 15 mW to 0.9 W [4], [5], [12].

Fig. 1(a) shows a typical circuit of the energy transmission system. This circuit can transmit power efficiently by applying a large voltage to the primary coil, which resonates the capacitances, C_1 and C_2, with inductances, L_1 and L_2, respectively. In this circuit, ω, $V_1, V_2, I_1, I_2, r_1, r_2, R_L$, and M show, respectively, the angular frequency, input and output voltages, input and output currents (primary and secondary coil currents, respectively), primary and secondary coil resistances, load for the capsule endoscope, and mutual inductance. The power from the power supply was transmitted to the secondary side *via* the primary coil, and supplied to the load R_L.

In previous studies, we found that high efficiency and high output power can be obtained with the following prototype coils at a frequency of 200–500 kHz [11]. Therefore, in the present study, we calculated SAR and current density as a function of frequency 100–700 kHz, with the coils described earlier [see Fig. 1(b)]. The primary coil had 14 turns ($L_1 = 100\ \mu$H, square), and the secondary coil had approximately 150 turns, wound around a ferrite core ($L_2 = 470\ \mu$H; ϕ: 5 mm × 18 mm; M = 2.0 μH, coupling coefficient k = 0.01 at a transmission distance of 10 cm). These coils were designed with consideration for the primary coil's current and transmission efficiency.

III. Specific Absorption Rate and Current Density

Generally, SAR is expressed by (1):

$$\mathrm{SAR} = \frac{\sigma E^2}{\rho} \tag{1}$$

where σ is the electrical conductivity of the biological tissue [in mho per meter (S/m)], E is the rms of the electric field (in volts per meter), and ρ is the density of the biological tissue (in kilogram per cubic meter). The SAR is evaluated by two methods [24], one experimental and one analytical. In the experimental method, the electric field in a liquid phantom is measured, but it is very difficult to measure accurately because the electric field sensor is too large and the resolution is too low. The second method, which is much easier to use, analyzes the distribution of electromagnetic fields. In this paper, SAR was analyzed numerically.

Current density J is expressed by (2):

$$J = \pi R f \sigma \mu H_{\mathrm{ave}} \tag{2}$$

where R is the radius of the loop for induced current (in meter) and μ is the magnetic permeability [in henry per meter (H/m)]. H_{ave} (in ampere per meter) is expressed by (3):

$$H_{\mathrm{ave}} = \frac{1}{R}\int_0^R H dR \tag{3}$$

where H is the rms of the magnetic field (in ampere per meter). Current density is evaluated by numerical analysis. The average value of the magnetic fields in the loop for induced current (H_{ave}) is obtained by substituting the magnetic field (H) as analyzed by an electromagnetic simulator for (3). Thus, current density J is obtained by substituting H_{ave} into (2).

SAR and current density have basic restrictions defined by the International Commission in Nonionizing Radiation Protection (ICNIRP) [25]. To protect against adverse effects on health, these basic restrictions should not be exceeded. In this research, basic restrictions for occupational exposure were employed [SAR $<$ 10 W/kg, $J < f$/100 mA], because a capsule endoscope with the energy transmission system is used in medical practice under the supervision of a physician. A value of SAR = 10 W/kg has been adopted by the IEEE standard (C 95.1, 2005) [26].

IV. Methods

A. Experimental Measurement of Electric and Magnetic Fields With the Biological Phantom

First, the electric and magnetic fields generated by the primary coil were measured and compared to the analytical values to determine whether the analytical values derived by the electromagnetic simulator were correct.

A signal oscillator (IWATSU, SG-4105), a high-speed amplifier (NF Electronic Instruments, 4025), and a capacitor for resonance (Evox Rifa, PHE450SB) are placed 700 mm from the primary coil on a nonconductive table at a height of 800 mm. The primary coil was placed 5 mm from a biological phantom that mimicked the electrical characteristics of biological tissue. The biological liquid phantom [27] composed of deionized water, polyethylene powder, sodium chloride, boric acid (Sigma Aldrich Japan), and the viscosity improver TX-151 (Anzai Commerce Corporation, Ltd.) was inserted into a circular polypropylene container (ϕ: 280 mm; height: 400 mm; thickness: 2 mm) and was used as a model of the human body [see Fig. 2(a)].

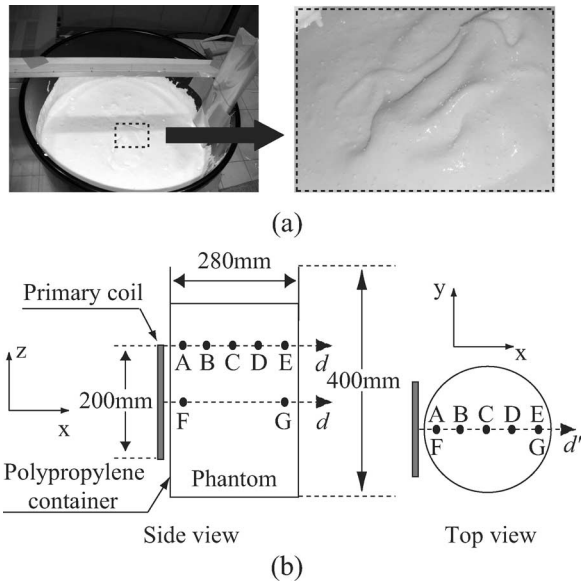

Fig. 2. (a) Biological phantom. (b) Measuring points.

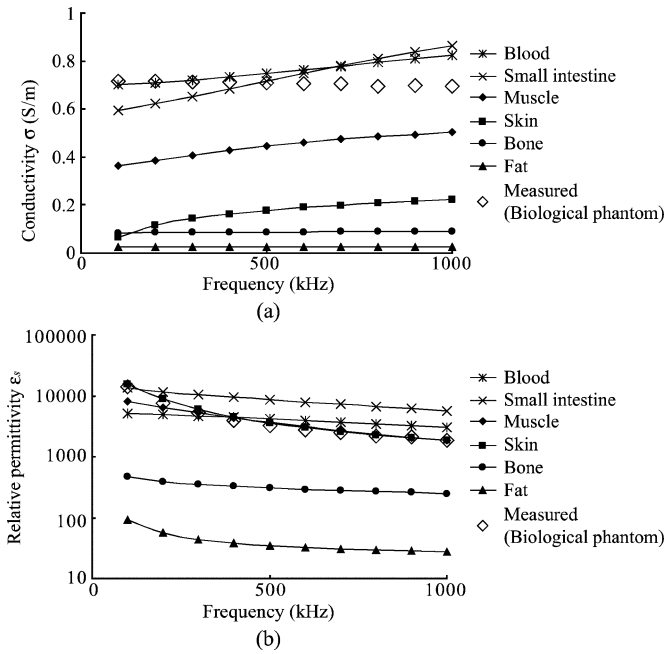

Fig. 3. Electrical characteristics of the biomedical tissue.

The conductivity σ and relative permittivity ε_s were measured to examine whether the electrical characteristics of the biological phantom were simulated correctly [28]. The electrical characteristics of the biological phantom are shown in Fig. 3 with diamonds. It was adjusted to be in the vicinity of those of the small intestine, blood, and muscle, which have large conductivity. The relative permittivity of three tissues are 2000–14 000 in this frequency range. These values were based on those reported by the Institute for Applied Physics (IFAC) [29], [30].

The electric fields E and magnetic fields H were measured with a frequency of 200 kHz and an output power of 0.9 W. The electric fields were measured with an electric field probe (Holaday, HI-4421G, isotropic deviation: $\pm$0.5 dB, linearity: $\pm$0.5 dB), and the magnetic fields were measured with a near field probe (Hewlett–Packard, 11941A, absolute error: $\pm$2 dB). The measurement points for the electric fields (around F and G; distance from primary coil, F: 5 cm and G: 25 cm) and magnetic fields (A–E: distance from primary coil, A: 5 cm, B: 10 cm, C: 15 cm, D: 20 cm, and E: 25 cm) are shown in Fig. 2(b). These measurements were taken in a radio anechoic chamber (W 2.6 m $\times$ H 2.6 m $\times$ L 6.6 m; Hiroshima Technoplaza) that had a shield performance of 80 dB at 150 kHz to 30 MHz.

B. Numerical Analysis of the Electric and Magnetic Fields, SAR and Current Density

To investigate the electromagnetic influence on biological tissue in more detail, we estimated SAR and current density as a function of frequency and output power by numerical analysis. This section explains the methods, models, and conditions used in the analyses.

1) Transmission-line modeling method: Microstripes (Flomerics, Japan Branch), an electromagnetic simulator employing the TLM method [20], was used for the analyses. The procedure of numerical analysis using microstripes is as follows. First, biological and electrical circuit models similar to the human configuration and electrical characteristics are created in the analytical space. This analytical space is then divided into small grid cells, and the magnetic field H, electric field E, and SAR are calculated for each grid cell. Then, the current density J is calculated from the magnetic field obtained by analysis using (2) and (3). This paper also analyzes SAR as a localized SAR, which is represented as an average value of 10 g of biological tissue. This corresponds to as many as about 68 cells measuring 3.9 mm $\times$ 3.9 mm $\times$ 9.7 mm.

2) Biological model for numerical analysis: Fig. 4 shows a biological model for numerical analysis. In Fig. 4(a), the trunk (abdominal part) of a human body is modeled as an elliptical cylinder with diameter 300 mm, and a primary coil (200 mm $\times$ 200 mm, 14 turns) is placed at a distance of 5 mm from the trunk. Fig. 4(b) shows the top view of the trunk model, which is composed of skin (thickness: 5 mm), fat (thickness: 10 mm), muscle (thickness: 15 mm), small intestine (ϕ 240 mm), blood (ϕ 20 mm), and backbone (ϕ 30 mm $\times$ 50 mm). The primary coil was arranged in α–γ, as shown in Fig. 4(c).

Fig. 3 shows the electrical characteristics of the biological tissue for numerical analysis. The figure shows the conductivity σ and the relative permittivity ε_s of the skin, fat, muscle, small intestine, blood, and backbone as a function of frequency. These values were based on those reported by the IFAC. In addition, an average value of 1000 kg/m^3 was used to represent the density of biological tissue consisting of skin, fat, muscle, small intestine, and blood, a value of 1850 kg/m^3 was used only for the backbone, and relative permeability was 1 [31], [32]. The analytical model was divided into 404 800 cells [cell size (near primary coil): x: 0.5 mm; y: 4 mm; z: 10 mm; others: x: 3.9 mm; y: 4 mm; z: 10 mm).

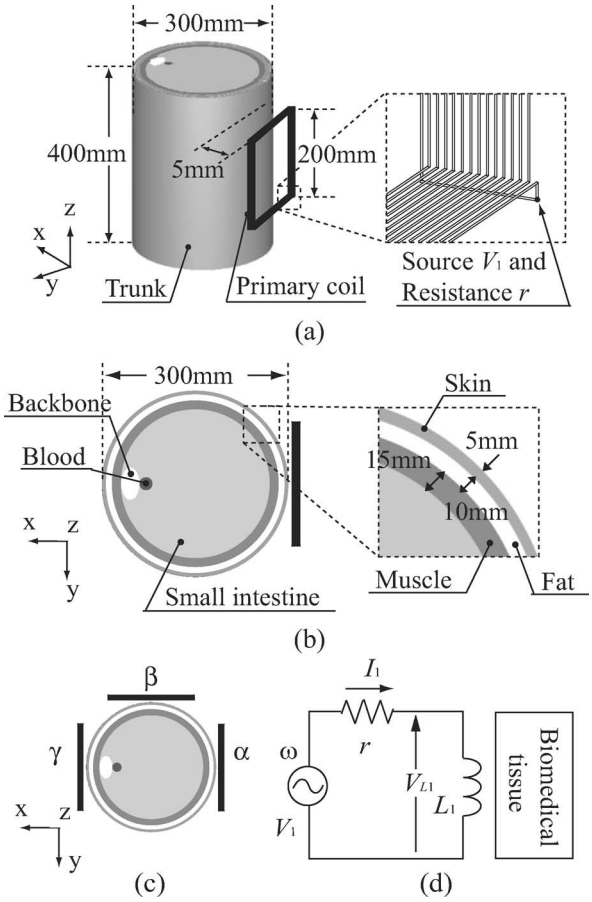

Fig. 4. (a) and (b) Analytical model (human body's trunk). (c) Arrangement of the primary coil. (d) Equivalent circuit for the analytical model.

3) Circuit model for the numerical analysis: The equivalent circuit of the analytical model is shown in Fig. 4(d). The primary coil current I_1 and the terminal voltage of the coil V_{L1} were adjusted by V_1 and R to be equal to the actual measurement values in the prototype coils. As analysis conditions, the frequency was varied between 100 and 700 kHz on output power of 0.01, 0.05, 0.1, 0.5, and 0.9 W (when $R_L = 10\ \Omega$).

V. Results

A. Experimental Measurement of Electric and Magnetic Fields With the Biological Phantom

Fig. 5(a) and (b) shows the measurements of the electric and magnetic fields, respectively. Here, all measured data are presented as means $\pm$ standard deviation (SD) ($n = 8$). The crosses show the simulated values. The electric field showed that the measurement values change because the size of the electric field probe is large and the position of the sensor is rotated. Then, we used the t-test to confirm whether the simulation values were within tolerance. The results confirmed that all the simulated data were within the 95% confidence interval ($P =$ 0.07 – 0.96).

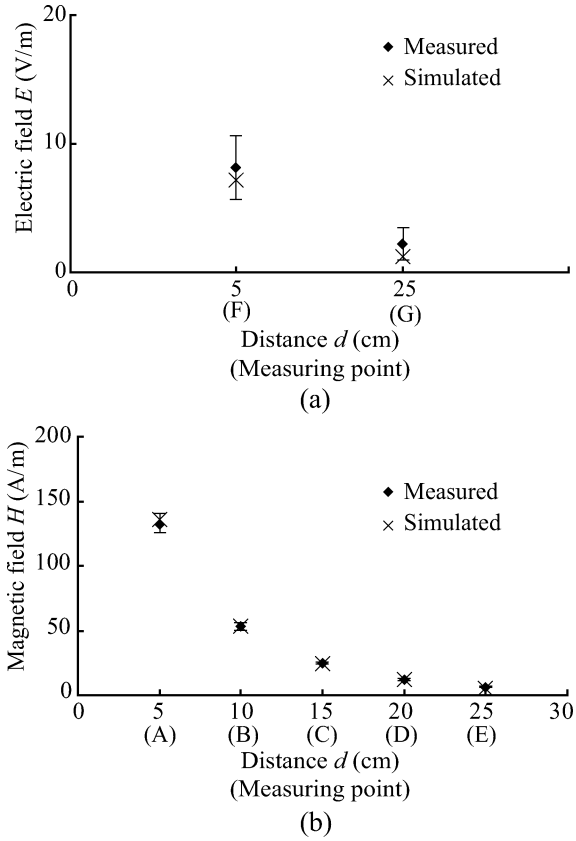

Fig. 5. Measurement and simulated results of the electric and magnetic fields.

B. Analysis of Localized SAR

At a frequency of 200 kHz and an output power of 0.1 W, the maximum SAR values for the arrangement of the primary coil (α–γ) were α: 12.2 mW/kg, β: 12.1 mW/kg, and γ: 11.2 mW/kg. From these results, the maximum SAR value appears in arrangement α. Therefore, the results for arrangement α are shown here.

The SAR distributions for a frequency of 200 kHz and output power of 0.9 W are shown in Fig. 6. Fig. 6(a) shows the SAR distribution of an x–z plane through the model's central axis, and Fig. 6(b) shows that of an x–y plane at $z = 0$. The results indicated that SAR was large on the inner side of the trunk's surface and was the maximum at point X, which is the part at the boundary of the muscle and small intestine.

Next, Fig. 7 shows the analytical results of the localized SAR on point X as a function of frequency when the output power was varied. Here, the dotted line indicates the ICNIRP basic restrictions on exposure. The plot shows that the localized SAR increased as the frequency and output power increased. The plot also shows that for every value of output power, it was possible to remain within the ICNIRP basic restrictions.

C. Analysis of Current Density

The magnetic field distributions at a frequency of 200 kHz and output power of 0.9 W are shown in Fig. 8. Fig. 8(a) shows the magnetic field distribution of an x–z plane through the model's central axis, and Fig. 8(b) shows the magnetic field distribution

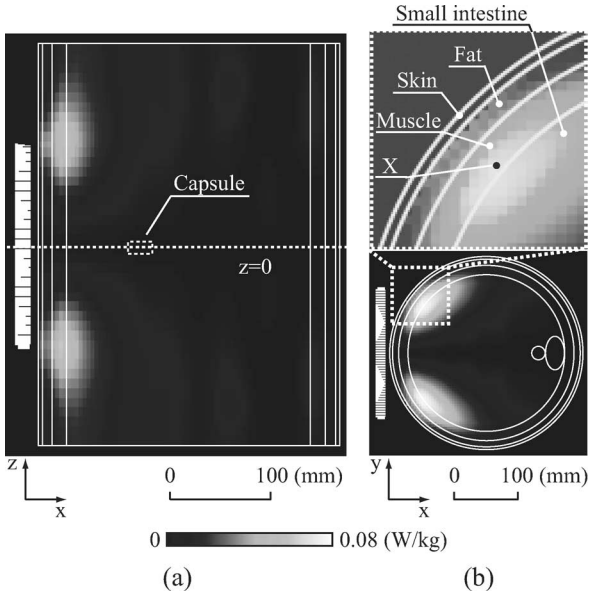

Fig. 6. Localized SAR distribution.

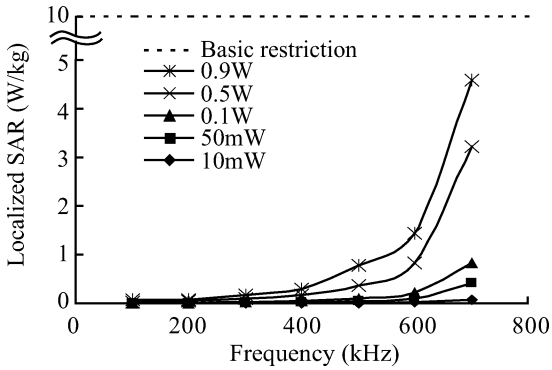

Fig. 7. SAR as a function of frequency.

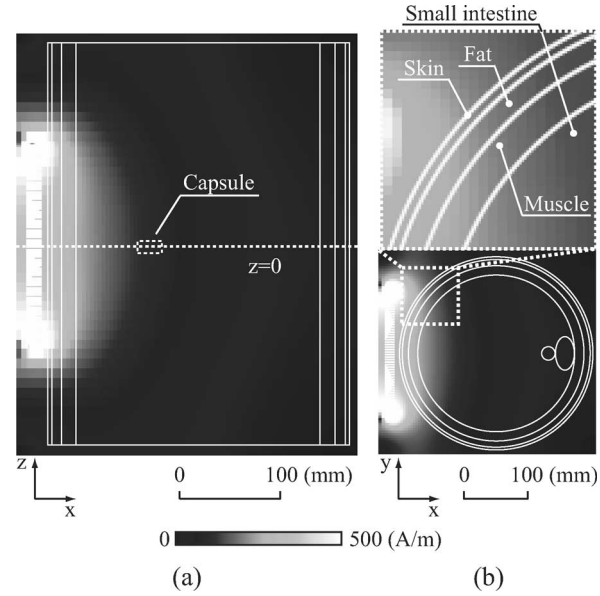

Fig. 8. Magnetic field distribution.

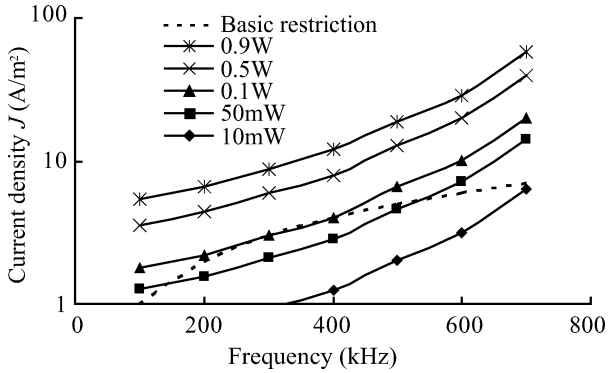

Fig. 9. Current density as a function of frequency.

of an x–y plane at $z = 0$. These results indicate that the magnetic field grew as the distance with the coil decreased. The current density was calculated from the magnetic field results, (2) and (3). At a frequency of 200 kHz and output power of 0.1 W, the maximum value for current density for arrangement α–γ of the primary coil was an equivalent value: 2.21 A/m^2. Therefore, the results for arrangement α are shown here.

Fig. 9 shows the analytical results of the maximum current density as a function of frequency when the output power was varied. Here, the dotted line indicates the ICNIRP basic restrictions. The plot shows that the current density increased as the frequency and output power increased. The plot also shows that the influences on biological tissue became smallest at 300–400 kHz when compared with the ICNIRP basic restrictions. Thus, it is possible to transmit power up to a maximum of 100 mW.

VI. Discussion

First, electric and magnetic fields generated by a primary coil were measured and compared to the simulated values to confirm whether the simulated values derived by the electromagnetic simulator were correct. Given the previous findings, the computed results were in good agreement with the experimental data. Therefore, the simulated results derived using the electromagnetic simulator appeared to be correct.

The SAR results showed that SAR was maximized in the boundary of muscle and the small intestine, and it increased as the frequency and output power increased. The results of SAR showed that it is possible to remain within the ICNIRP basic restrictions for every value of output power from 10 mW to 0.9 W.

Fig. 10 shows the measurement results of the terminal voltage of the prototype primary coil V_{L1} with an output power of 0.9 W. V_{L1} is equal to the terminal voltage of the resonant capacitance V_{C1} at the resonant frequency. A comparison of the plots shown in Fig. 7 with Fig. 10 shows that the SAR was dependent on the terminal voltage of the primary coil. Therefore, to develop an energy transmission system that involves SAR, it is necessary to reduce the terminal voltage of the primary coil by designing the opposite configuration and size of coils because the terminal voltage is essentially proportional to the square root of coil inductance rate L_1/L_2 and secondary coil resistance r_2 [11].

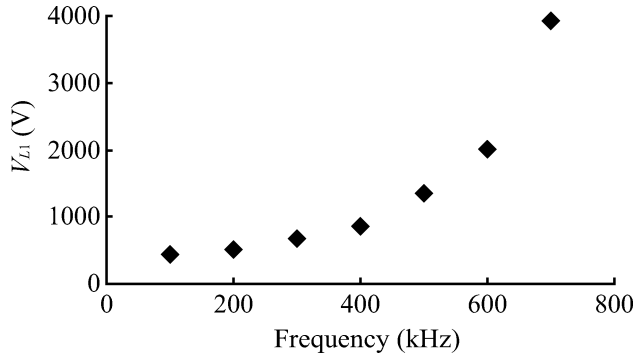

Fig. 10. Measurement results of the terminal voltage of the primary coil.

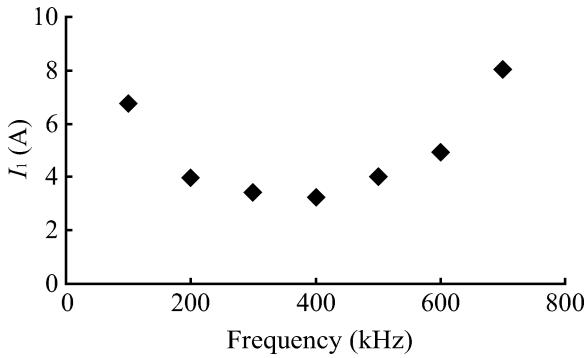

Fig. 12. Measurements of the primary coil current.

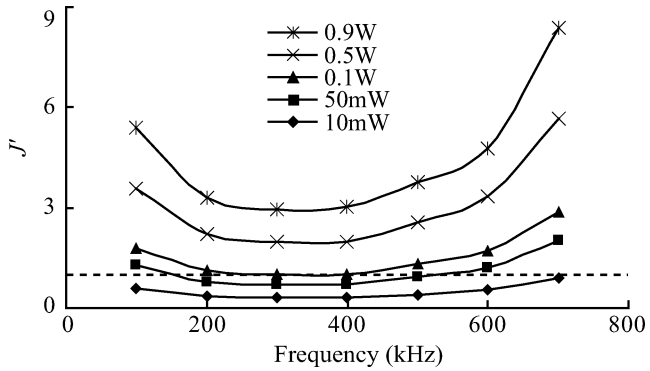

Fig. 11. Normalized current density J' as a function of frequency.

The results showed that current density increased as frequency and output power increased. Moreover, the influences on biological tissue became smallest at 300–400 kHz as compared with the ICNIRP basic restrictions. Thus, it is possible to transmit power up to a maximum of 100 mW.

Fig. 11 shows the normalized current density J', which is divided by the ICNIRP basic restrictions in Fig. 9. Fig. 11 shows that if $J' \leq 1$, the current density remains within the ICNIRP basic restrictions. In addition, the measurement results of the primary coil current I_1 with an output power of 0.9 W are shown in Fig. 12. The plot in Fig. 11 corresponds with that in Fig. 12, suggesting that the current density depends on the current in the primary coil. This is a reasonable result, because the primary coil current I_1 is proportional to H, which is known to be a cause of current density J. Therefore, to transmit more power safely, it is necessary to reduce the current density by reducing the primary coil current I_1.

Here, the primary coil current I_1 is expressed by (4) [11]

$$I_1 = \frac{(r_2 + R_L)\, P_0^{1/2}}{\omega M R_L^{1/2}} \tag{4}$$

where P_0 and R_L are output power and load resistance, respectively (both of which are constant). Using (4), we devised the following methods to reduce the current density by reducing the primary coil current: 1) enlarging the mutual inductance M, or 2) reducing the secondary coil resistance r_2.

For method (1), the easiest way to enlarge M is to enlarge the number of turns in the coil. However, increasing the number of turns in the primary coil, n_1, is not an effective method, because the current density J is dependent on not only I_1, but also on n_1 ($J \infty n_1 I_1$) when n_1 is not constant. Therefore, the current density J does not change, even if the number of turns in the primary coil, n_1, increases. In addition, it is difficult to enlarge the number of turns in the secondary coil, n_2, considering the size of the secondary coil.

On the other hand, method (2) is possible. Changing the conventional winding wire (UEW wire, ϕ: 0.1 mm; cross-sectional area: 0.0078 mm^2) to Litz wire (UEW wire, bundles of 15 wires of ϕ: 0.03 mm (ϕ: 0.13 mm); cross-sectional area: 0.0106 mm^2) decreases the secondary coil resistance r_2 by 22.5%–24.5%, which decreases the input current I_1 by 8.2%–20.2% and the current density by 8.1%–20.9% (at a frequency of 200–400 kHz and an output power of 0.9 W). In addition, it was confirmed that it is possible to transmit power up to a maximum of 160 mW below the ICNIRP basic restrictions at a frequency of 400 kHz. Therefore, the design of an energy transmission system to reduce the primary coil current I_1 is important.

The wireless capsule endoscope, which is a commercially available system, has frame restraints and operating time limitations for filming (2 frames/s for 8 h with power consumption of about 15 mW) imposed by the use of internal batteries. On the other hand, the results of the present study indicated that it is possible to transmit power of up to 160 mW. Thus, it is estimated that it is possible to take detailed pictures of at least 21 frames/s [=2 frames $\times$ (160 mW/15 mW)].

In this paper, the relative position and direction of the secondary coil to the primary coil were fixed where the maximum power was transmitted. However, the position and direction of the secondary coil cannot be uniquely determined inside the human body. In future, we will use three coils in the x, y, and z directions and pass the current through only the highest coupling primary coil to suppress the increase in transmitting power and electromagnetic influence caused by the position and direction of the secondary coil.

VII. Conclusion

In this paper, we analyzed SAR and current density in the biological tissue surrounding the primary coil of an energy transmission system for a wireless capsule endoscope, and examined the transmission conditions needed to reduce the

electromagnetic influence on biological tissue. The results showed that the SAR remains within the ICNIRP basic restrictions for every value of output power from 10 mW to 0.9 W at frequencies of 100–700 kHz, and the current density was smallest at 300–400 kHz; thus, it is possible to transmit power up to a maximum of 160 mW. Our results also confirmed that it is possible to reduce the current density by reducing the secondary coil resistance, which opens the possibility of extending the maximum transmission power. In future, we will analyze the SAR and current density using a more precise human model, such as MRI-based models, and will perform the analyzes with transmission distances of 200 mm, 300 mm, and more. In addition, it will be necessary to design an energy transmission system taking both safety and performance into consideration.

ACKNOWLEDGMENT

The authors would like to thank Y. Hasegawa and N. Kuwano (Flomerics, Japan Branch) for their useful suggestions and assistance with regard to the electromagnetic simulator.

REFERENCES

[1] G. Iddan, G. Meron, A. Glukhovsky, and P. Swain, "Wireless capsule endoscopy," *Nature*, vol. 405, no. 6785, pp. 417–417, 2000.

[2] Olympus launches high-resolution capsule endoscope in Europe—The capsule endoscope system for small bowel which allows real time observation-. Olympus Corporation, Tokyo, Japan. [Online]. Available: http://www.olympus-global.com/en/news/2005b/nr051013capsle.cfm?chm=4.

[3] D. G. Adler and C. J. Gostout, "Wireless capsule endoscopy," *Hosp. Physician*, pp. 14–22, May 2003.

[4] X. Xie, G. L. Li, B. Y. Chi, X. Y. Yu, C. Zhang, and Z. H. Wang, "Microsystem design for wireless endoscopy system," in *Proc. IEEE, Eng. Med. Biol. 27th Ann. Conf.*, Shanghai, China, Sep. 2005, pp. 7135–7138.

[5] The American Society for Gastrointestinal Endoscopy, "ASGE technology status evaluation report: Wireless capsule endoscopy," *Gastrointest. Endosc.*, vol. 63, no. 4, pp. 539–549, 2006.

[6] H. J. Park, J. C. Park, J. H. Lee, Y. K. Moon, B. S. Song, C. H. Won, H. C. Choi, J. T. Lee, and J. H. Cho, "New method of moving control for wireless endoscopic capsule using electrical stimulus," *IEICE Trans. Fundam. Electron., Commun. Comput. Sci.*, vol. E88-A, pp. 1476–1480, 2005.

[7] A. Ali, J. M. Santisi, and J. Vargo, "Video capsule endoscopy: A voyage beyond the end of the scope," *Cleve. Clin. J. Med.*, vol. 71, no. 5, pp. 415–425, 2004.

[8] L. Aabakken, "Capsule endoscopy is feasible in small children," *Endoscopy*, vol. 35, p. 789, 2003.

[9] B. Lenaerts and R. Puers, "Inductive powering of a freely moving system," *Sens. Actuators A*, vol. 123/124, pp. 522–530, 2005.

[10] S. W. Lee, J. D. Kim, J. H. Son, M. H. Ryo, and J. Kim, "Design of two-dimensional coils for wireless power transmission to in vivo robotic capsule," in *Proc. IEEE, Eng. Med. Biol. 27th Ann. Conf.*, Shanghai, China, Sep.2005, pp. 6631–6634.

[11] A. Morimasa, T. Nagato, K. Shiba, and T. Tsuji, "Energy transmission system for endoscopy capsule—An attempt to improve the transmission ability," in *Proc. Soc. Life Support Technol. 21th Ann. Conf.*, Mie, Japan, Dec.2005, p. 11.

[12] K. Inagaki and K. Koshiji, "Investigation of transcutaneous energy transmission system for a capsuled camera inside the body," in *Proc. 17th Symp. Electromagn. Dyn.*, Kochi, Japan, Jun.2005, pp. 22–24.

[13] A. Hirata, H. Watanabe, and T. Shiozawa, "SAR and temperature increase in the human eye induced by obliquely incident plane waves," *IEEE Trans. Electromagn. Compat.*, vol. 44, no. 4, pp. 592–594, Nov. 2002.

[14] K. Fukunaga, S. Watanabe, and Y. Yamanaka, "Dielectric properties of tissue-equivalent liquids and their effects on specific absorption rate," *IEEE Trans. Electromagn. Compat.*, vol. 46, no. 1, pp. 126–129, Feb. 2004.

[15] J. C. Schuder, "Powering an artificial heart: Birth of the inductively coupled-radio frequency system in 1960," *Artif. Organs*, vol. 26, no. 11, pp. 909–915, 2002.

[16] K. Shiba, E. Shu, K. Koshiji, K. Tsukahara, K. Tsuchimoto, T. Ohumi, T. Nakamura, S. Endo, T. Masuzawa, E. Tatsumi, Y. Taenaka, and H. Takano, "Efficiency improvement and in vivo estimation of externally-coupled transcuteneous energy transmission system for a totally implantable artificial heart," in *Proc. 19th Ann. Int. Conf. IEEE Eng. Med. Biol. Soc.*, 1997, pp. 2503–2505.

[17] K. Shiba, K. Koshiji, E. Tatsumi, Y. Taenaka, and H. Takano, "Analysis of specific absorption rate in biological tissue surrounding transcutaneous transformer for an artificial heart," *J. Artif. Organs*, vol. 5, no. 2, pp. 91–96, 2002.

[18] K. Shiba, M. Nukaya, T. Tsuji, and K. Koshiji, "Analysis of current density and specific absorption rate in biological tissue surrounding an air-core type of transcutaneous transformer for an artificial heart," in *Proc. IEEE 2006 Int. Conf. Eng. Med. Biol. Soc.*, pp. 5392–5395.

[19] S. Ueno and K. Harada, "Experimental difficulties in observing the effects of magnetic fields on biological and chemical processes," *IEEE Trans. Magn.*, vol. 22, no. 5, pp. 868–873, Sep. 1986.

[20] C. Christos, *The Transmission-Line Modeling Method*. New York: IEEE Press, 1995.

[21] P. B. Johns, "A symmetrical condensed node for the TLM method," *IEEE Trans. Microw. Theory Tech.*, vol. MTT-35, no. 4, pp. 370–377, Apr. 1987.

[22] V. Trenkic, C. Christopoulos, and T. M. Benson, "Optimization of TLM schemes based on the general symmetrical condensed node," *IEEE Trans. Antennas Propag.*, vol. 45, no. 3, pp. 457–465, Mar. 1997.

[23] A. J. Wlodarczyk, V. Trenkic, R. A. Scaramuzza, and C. Christopoulos, "A fully integrated multiconductor model for TLM," *IEEE Trans. Microw. Theory Tech.*, vol. 46, no. 12, pp. 2431–2437, Dec. 1998.

[24] S. Nitta, Y. Kami, Y. Sato, K. Sugiura, N. Seto, and O. Fujiwara, *Electromangetic Compatibility Handbook*. Tokyo, Japan: Asakura Publishers, 1999.

[25] International Commission on Non-Ionizing Radiation Protection, "Guidelines for limiting exposure to time-varying electric, magnetic, and electromagnetic fields (up to 300 GHz)," *Health Phys.*, vol. 74, no. 4, pp. 494–522, 1998.

[26] IEEE International Committee on Electromagnetic Safety (SCC39), *IEEE standard for safety levels with respect to human exposure to radio frequency electromagnetic fields, 3 kHz to 300 GHz,* IEEE Standard C95.1, pp. 18–21, 2005.

[27] Y. Okano, K. Ito, I. Ida, and M. Takahashi, "The SAR evaluation method by a combination of thermographic experiments and biological tissue-equivalent phantoms," *IEEE Trans. Microw. Theory Tech.*, vol. 48, no. 11, pp. 2094–2103, 2000.

[28] K. Shiba and K. Koshiji, "Electromagnetic compatibility of transcutaneous energy transmission system for totally implantable artificial heart," *IEEJ Trans. Electron., Inf. Syst.*, vol. 123, no. 7, pp. 1219–1227, 2003.

[29] C. Gabriel, S. Gabriel, and E. Corthout, "The dielectric properties of biological tissues: I. Literature survey," *Phys. Med. Biol.*, vol. 41, pp. 2231–2249, 1996.

[30] S. Gabriel, R. W. Lau, and C. Gabriel, "The dielectric properties of biological tissues: II. Measurements in the frequency range 10 Hz to 20 GHz," *Phys. Med. Biol.*, vol. 41, pp. 2251–2269, 1996.

[31] Japan Society of Medical Electronics and Biological Engineering, *Handbook of Clinical Engineering*. Tokyo, Japan: Corona Publishers, 1984, p.113.

[32] G. Luo, J. J. Kaufman, A. Chabrera, B. Bianco, J. H. Kinney, D. Haupt, J. T. Ryaby, and R. S. Siffert, "Computational methods for ultrasonic bone assessment," *Ultrasound Med. Biol.*, vol. 25, pp. 823–830, 1999.

Kenji Shiba (M'00) received the B.E., M.E., and D.E. degrees in electrical engineering from Tokyo University of Science, Chiba, Japan, in 1995, 1997, and 2000, respectively.

From 2000 to 2001, he was a Research Fellow at Japan Society for the Promotion of Science. During 2001, he was with the Department of Human and Engineered Environmental Studies, University of Tokyo, Tokyo, Japan, as a Research Associate. During 2002, he was with Tokyo University of Science as a Research Associate. Since 2004, he has been with the Department of Artificial Complex Systems, Hiroshima University, Higashi-Hiroshima, Japan, where he is currently an Associate Professor. His current research interests include implantable medical devices, bioelectromagnetics, and electromagnetic compatibility.

Prof. Shiba is a member of the IEEE Engineering in Medicine and Biology Society, the IEEE Electromagnetic Compatibility Society, the Japanese Society for Artificial Organs (JSAO), the Society of Life Support Technology, the Japan Society of Mechanical Engineers, and the Japan Society of Medical Electronics and Biological Engineering. He was the recipient of the Best Paper Award from the Japanese Society for Artificial Organs in 2001.

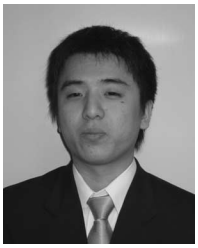

Tomohiro Nagato received the B.E. degree in electrical, computer, and systems engineering in 2005, and the M.E. degree in artificial complex systems engineering in 2007, both from Hiroshima University, Higashi-Hiroshima, Japan.

He is currently at Hiroshima University. His current research interest includes transcutaneous energy transmission system for a wireless capsule endoscope.

Toshio Tsuji (A'88–M'99) received the B.E. degree in industrial engineering in 1982, the M.E. and Doctor of Engineering degrees in systems engineering in 1985 and 1989, respectively, all from Hiroshima University, Higashi-Hiroshima, Japan.

Since 1985, he has been with the Faculty of Engineering, Hiroshima University, earlier as a Research Associate, and later, an Associate Professor, and currently, a Professor in the Department of Artificial Complex Systems Engineering. From 1992 to 1993, he was a Visiting Professor at the University of Genova, Italy. His current research interests include human–machine interface and computational neural sciences, in particular, biological motor control.

Prof. Tsuji is a member of the Institute of Electrical and Electronics Engineers, the Japan Society of Mechanical Engineers, the Robotics Society of Japan, and the Society of Instrumentation and Control Engineers in Japan. He is the recipient of the Best Paper Award from the Society of Instrumentation and Control Engineers in 2002, and the K. S. Fu Memorial Best Transactions Paper Award of the IEEE Robotics and Automation Society in 2003.

Kohji Koshiji (M'91) received the D.E. degree in 1978 from the Department of Electrical Engineering, Tokyo University of Science, Chiba, Japan.

He is currently a Professor in the Department of Electrical Engineering, Tokyo University of Science. His current research interests include biomedical engineering, biomaterial studies, analysis and design of microwave circuit, and analysis and design of electronic equipment considering electromagnetic compatibility.

Prof. Koshiji is a member of the IEEE Engineering in Medicine and Biology Society, the IEEE Electromagnetic Compatibility Society, the Institute of Electronics, Information and Communication Engineers (IEICE), the Japanese Society for Artificial Organs (JSAO), and the American Society for Artificial Internal Organs (ASAIO).